IOP Publishing Superconductor Science and Technology
Supercond. Sci. Technol. **28** (2015) 075009 (9pp) doi:10.1088/0953-2048/28/7/075009

Numerical modelling and comparison of MgB_2 bulks fabricated by HIP and infiltration growth

J Zou[1], M D Ainslie[1], H Fujishiro[2], A G Bhagurkar[3], T Naito[2], N Hari Babu[3], J-F Fagnard[4], P Vanderbemden[4] and A Yamamoto[5]

[1] Bulk Superconductivity Group, Department of Engineering, University of Cambridge, Trumpington Street, Cambridge CB2 1PZ, UK
[2] Department of Materials Science and Engineering, Faculty of Engineering, Iwate University, 4-3-5 Ueda, Morioka 020-8551, Japan
[3] Brunel Centre for Advanced Solidification Technology, Brunel University, Uxbridge UB8 3PH, UK
[4] SUPRATECS and Department of Electrical Engineering and Computer Science B28, Sart-Tilman, B-4000 Liege, Belgium
[5] Department of Applied Chemistry, University of Tokyo, 7-3-1 Hongo, Bunkyo-ku, Tokyo 113-8656, Japan

E-mail: mda36@cam.ac.uk

Received 2 March 2015, revised 28 April 2015
Accepted for publication 30 April 2015
Published 26 May 2015

Abstract

MgB_2 in bulk form shows great promise as trapped field magnets (TFMs) as an alternative to bulk (RE)BCO materials to replace permanent magnets in applications such as rotating machines, magnetic bearings and magnetic separation, and the relative ease of fabrication of MgB_2 materials has enabled a number of different processing techniques to be developed. In this paper, a comparison is made between bulk MgB_2 samples fabricated by the hot isostatic pressing (HIP), with and without Ti-doping, and infiltration growth (IG) methods and the highest trapped field in an IG-processed bulk MgB_2 sample, $B_z = 2.12$ at 5 K and 1.66 T at 15 K, is reported. Since bulk MgB_2 has a more homogeneous J_c distribution than (RE)BCO bulks, studies on such systems are made somewhat easier because simplified assumptions regarding the geometry and J_c distribution can be made, and a numerical simulation technique based on the 2D axisymmetric $\boldsymbol{H}$-formulation is introduced to model the complete process of field cooling (FC) magnetization. As input data for the model, the measured $J_c(B,T)$ characteristics of a single, small specimen taken from each bulk sample are used, in addition to measured specific heat and thermal conductivity data for the materials. The results of the simulation reproduce the experimental results extremely well: (1) indicating the samples have excellent homogeneity, and (2) validating the numerical model as a fast, accurate and powerful tool to investigate the trapped field profile of bulk MgB_2 discs of any size accurately, under any specific operating conditions. Finally, the paper is concluded with a numerical analysis of the influence of the dimensions of the bulk sample on the trapped field.

Keywords: bulk MgB_2, numerical modelling, hot isostatic pressing, infiltration growth, trapped field magnets, field cooling, superconductivity

(Some figures may appear in colour only in the online journal)

1. Introduction

Large, single-grain (RE)BCO (where RE = rare earth element or yttrium) bulk superconductors have significant potential to trap large magnetic fields over 17 T at temperatures below 30 K [1, 2] and up to 3 T at the technologically important temperature of 77 K [3]. Such materials fabricated into disc shapes are typical candidates to replace permanent magnets in applications such as rotating machines [4], magnetic bearings [5–7] and magnetic separation [8]. The field trapping ability of these materials depends critically on the capability to maintain a high critical current density (J_c) in the presence of large magnetic fields [9], a large shielding current loop, and a well-aligned grain microstructure [10]. However, (RE)BCO bulk superconductors can unfortunately suffer from an inhomogeneous J_c distribution during the growth process and it is difficult to fabricate large, single-domain (RE)BCO bulk superconductors with homogeneous properties over 100 mm in diameter [11].

Superconductivity in MgB_2 was first reported in 2001 in [12]. Although the critical temperature, T_c, for this material is low (39 K), requiring a lower operating temperature (15–20 K), which can lead to thermal instability/flux jumps, and a more complex cryogenic system than that required for (RE)BCO bulks, the material is cheaper, lighter weight and has a more homogeneous J_c distribution. Hence, MgB_2 in bulk form shows great promise as trapped field magnets (TFMs) as an alternative to (RE)BCO materials.

The relative ease of fabrication of MgB_2 materials, as well as their long coherence length [13], lower anisotropy and strongly linked supercurrent flow in untextured polycrystalline samples [14, 15], has enabled a number of different processing techniques to be developed. Significant improvements continue to be made in terms of in-field J_c and trapped field capability:

- 5.4 T at 12 K was achieved in a single 20 mm diameter MgB_2 bulk fabricated by hot-pressing ball-milled Mg and B powders [16];
- 4 T at 11 K and 3 T at 20 K with a pair of 30 mm diameter MgB_2 bulks fabricated by conventional *in situ* reaction [17];
- 3.6 T at 13.2 K and 2.8 T at 20 K with a single 38 mm diameter Ti-doped MgB_2 bulk fabricated by the hot isostatic pressing (HIP) method [18];
- 3.14 T at 17.5 K with a pair of 25 mm diameter MgB_2 bulks fabricated by uniaxial hot pressing [19];
- 1.5 T at 16.4 K with a 30 mm diameter MgB_2 bulk fabricated by a capsule method [20]; and
- 1.3 T at 15 K with a 55 mm diameter sample (with a 6 mm central hole) fabricated by the reactive Mg liquid infiltration (Mg-RLI) technique [21].

In this paper, a comparison is made between bulk MgB_2 samples fabricated by the HIP and infiltration growth (IG) methods and the highest trapped field in an IG-processed bulk MgB_2 sample is reported. A numerical simulation technique based on the 2D axisymmetric $\boldsymbol{H}$-formulation is then introduced to model the complete process of field cooling (FC) magnetization. As input data for the model, the measured $J_c(B,T)$ characteristics of a single, small specimen taken from each bulk sample are used, in addition to measured specific heat and thermal conductivity data for the materials, and the results of the simulation reproduce the experimental results extremely well. The numerical model provides a fast, accurate and powerful tool to investigate the trapped field profile of bulk MgB_2 discs of any size accurately, under any specific operating conditions. Finally, the diameter and thickness dependence of the trapped field profile is assessed with a view of optimizing the geometry of the bulks for such materials acting as TFMs in practical applications.

2. Sample fabrication and properties

2.1. HIP method

Three MgB_2 bulk superconductors were prepared using a HIP method [11], which are annotated as HIP#22, HIP#38 and HIP-Ti20% in this paper. The HIP#22 and HIP#38 samples were fabricated as described in [11], where a precursor pellet was prepared by cold isostatic pressing at 196 MPa using mixed powders of Mg (99.5% purity, $\leqslant$180 μm grain size), and B (99% purity, $\leqslant$50 μm grain size) with a molar ratio of 1.0:2.0. For the HIP-Ti20% sample, Ti (99% purity, $\leqslant$45 μm grain size) was added to the Mg and B powders with a molar ratio of Ti:Mg:B = 0.2:0.8:2.0, and then the precursor pellet was prepared. In the HIP-Ti20% sample, a small amount of Ti is reacted and substituted for the Mg-site and, as a result, most of the Ti is precipitated as a metal Ti phase [18]. All of these pellets were sealed under vacuum in a stainless steel container and were heated at 900 °C for 3 h under an isostatic pressure of 98 MPa. The samples were then embedded in a stainless steel ring, prepared especially for FC magnetization with a slightly larger inner diameter than the sample, using epoxy resin (Stycast 2850^{TM}). The outer diameter of the ring was fixed as 65 mm for all the three samples to match the cold head and each sample was tightly anchored onto a cold stage of a Gifford–McMahon cycle helium refrigerator for FC magnetization.

2.2. IG method

For the IG processed samples, crystalline boron powder (98% purity, <38 μm particle size, phase: rhombohedral) and sub-μm MgB_2 powder (Pavezyum) were thoroughly mixed with a ratio (by weight) of 70:30. The resultant mix of powders was used to make a cylindrical precursor (32 mm diameter, 6 mm thickness) under a uniaxial load of 10 MPa and the inclusion of the MgB_2 powder in the precursor allows for improvement of the wettability of the system. Magnesium was separately melted and held at 700 °C in a graphite crucible. The precursor was kept in a porous steel enclosure, which was then slowly transferred to the crucible containing liquid Mg. The use of the porous steel enclosure ensures that no part of the precursor touches the walls of the crucible and that it does not float on top of the Mg melt, which can result in non-uniform

infiltration. Boron has poor wetting with liquid Mg. This, together with a 25% volume shrinkage in the MgB_2 phase formation, can also result in non-uniform infiltration, which can lead to further defects, such as continuous Mg channels (as the MgB_2 phase begins to form in the precursor pellet, the resulting shrinkage makes way for the surrounding liquid Mg [22]). Such samples have very low trapped fields as the concentric current loops that form in a type II superconductor are impeded by these non-superconducting Mg channels. Thus, wettability of the precursor is important to obtain homogeneous infiltration. In this sample, a fraction of pre-synthesized MgB_2 powder is used as a wetting enhancer (mixed thoroughly with Boron), so continuous Mg channels are eliminated.

The assembly is then subject to the thermal profile shown in [22] and reacted at 850 °C for four hours. A cover gas mixture of $N_2 + SF_6$ with a volume ratio of 95:5 was maintained to minimize oxidation of the Mg. The SF_6 gas is significantly denser than air/oxygen and is also inert towards liquid Mg; thus, a continuous flow of this gas ensures formation of a layer of SF_6-rich atmosphere on the surface of the Mg melt and protects the melt from oxidation. After the reaction is complete, the surrounding Mg was removed by machining and the sample was recovered.

2.3. Sample information

After the initial FC magnetization trapped field measurements were carried out, a small, rectangular prism-shaped specimen was taken from each bulk sample (approximately $1 \times 1 \times 2\ mm^3$ in size from the HIP samples and $2 \times 2 \times 3\ mm^3$ from the IG sample) to measure the $J_c(B,T)$ characteristics. Magnetization curve M(H) measurements at 10 K, 20 K and 30 K (5 K, not 10 K, for the IG sample) were carried out using a commercial SQUID magnetometer (MPMS-5T). The $J_c(B,T)$ characteristics were estimated from the M(H) hysteresis loop by employing the extended Bean model [23]. Detailed information on all of the samples under analysis is provided in table 1.

In order to make a fair and adequate comparison between all of the samples made by the HIP and IG processes, a correction factor is used to normalize the measured trapped fields $B_z(T)$ for the samples due to their different dimensions. Similar to the method used in [16, 24], the measured trapped fields were normalized to consider the bulk (or average), in-field critical current density for each sample, averaged over the sample volume. The original, measured trapped field is divided by the factor, $-k\mu_0 a$, as given by equation (1), where k is the geometric constant given by equation (2) to account for different sample radii and thicknesses:

$$B_{trap} = k\mu_0 J_c R, \tag{1}$$

$$k = \frac{t_B}{2R} \cdot \ln\left(\frac{R + \sqrt{R^2 + {t_B}^2}}{t_B}\right), \tag{2}$$

where R and t_B are the sample radius and thickness, respectively. The normalized results for the temperature dependence of the average, in-field critical current density for each sample are shown in figure 1. For the reader's reference, the original, raw trapped field data is presented in section 3.2 (figure 7), where a comparison is made with the simulated results from the numerical model. From figure 1, it can be observed that among the three HIP samples, HIP-Ti20% has, as well as a higher trapped field, the highest normalized J_c, indicating the positive effect the Ti-doping has on improving the superconducting properties of HIP samples [18]. Although the IG sample has a comparatively lower trapped field/J_c in comparison with the HIP samples, its trapped field is the highest reported to date, and the IG process offers significant advantages due to its lower reaction temperature and capability to produce large samples in polycrystalline form of different shapes that can carry large current, and hence, provide large trapped fields [25].

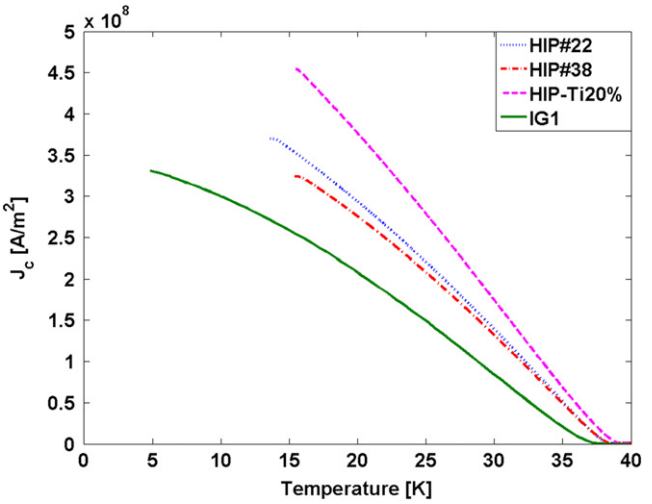

Figure 1. Temperature dependence of the normalized, average in-field critical current density J_c calculated for each bulk MgB_2 sample under analysis.

3. Numerical simulation of FC magnetization

The development of appropriate, practical magnetization techniques is crucial to the success of bulk superconductors acting as TFMs in practical applications, and there are three main methods of magnetization in common use: zero field cooling (ZFC), FC and pulsed field magnetization (PFM) [24]. In ZFC, the temperature of bulk samples is lowered down below their critical temperature, T_c, before the application and removal of the external magnetizing field. The field required to trap the maximum possible field with the FC method, where the superconductor is cooled below T_c in the presence of the external field, is half of the field required for ZFC. The PFM technique can be considered a type of ZFC, but the duration of the applied magnetic pulse is very short, on the order of milliseconds [26]. Compared with ZFC and FC techniques, the PFM technique provides a compact, mobile and relative inexpensive way to magnetize the bulk samples. However, the trapped field produced by PFM is generally much smaller than the other two techniques because

Table 1. Bulk MgB_2 sample information.

Sample	HIP#22	HIP#38	HIP-Ti20%	IG1
T_c (K)	38.5	38.5	39	37.5
Diameter, d (mm)	22	38	36	32
Thickness, t_B (mm)	18	7	7	6
Aspect ratio (d/t_B)	1.2	5.4	5.1	5.33
Relative mass density	93%	93%	94%	90%
Maximum trapped field, B_z (FC at 20 K) (T)	1.92	2.09	2.77	1.34
J_c (FC at 20 K) (A m^{-2})[a]	2.94×10^8	2.76×10^8	4.23×10^8	2.08×10^8
Reference	[11]	[11]	[11]	[22]

[a] Calculated from the measured trapped fields presented in figure 7 using equations (1) and (2).

of the significant temperature rise generated by fast magnetic flux propagation during this magnetizing process [27]. In this section, a numerical modelling technique is introduced to model the complete process of FC magnetization.

In practical applications of superconducting materials in which changes in temperature are non-trivial, such as the PFM of bulks, temperature-dependent modelling is inevitable to simulate accurate temperature, current and magnetic field distributions. Numerical simulation is also a powerful tool to optimize the design of the magnetization fixture and determine the optimal activation field when using various magnetization techniques [28]. The more homogeneous J_c distribution of bulk MgB_2 makes studies on such systems somewhat easier because simplified assumptions can be made regarding the geometry and the J_c distribution in comparison to (RE)BCO bulks, i.e., a 2D axisymmetric model can be used and the assumptions regarding J_c are less dependent on the position of sub-specimens taken from the sample [28, 29].

3.1. Modelling framework and assumptions

The numerical model developed here combines the electromagnetic and thermal equations governing the behaviour of the superconducting material, based on the 2D axisymmetric $\boldsymbol{H}$-formulation [30–32] implemented using the commercial FEM software package COMSOL Multiphysics 4.3a. The ac/dc module of COMSOL is employed for the electromagnetic analysis and the Heat Transfer module is used for the thermal analysis, which are coupled together as described below and in [24]. A schematic view of the numerical model, including the cold head and vacuum chamber, is shown in figure 2.

In the 2D axisymmetric $\boldsymbol{H}$-formulation, the governing equations are derived from Maxwell's equations—namely, Faraday's (3) and Ampere's (4) laws:

$$\nabla\times\boldsymbol{E}+\frac{\mathrm{d}\boldsymbol{B}}{\mathrm{d}t}=\nabla\times\boldsymbol{E}+\frac{\mathrm{d}\left(\mu_0\mu_r\boldsymbol{H}\right)}{\mathrm{d}t}=0, \tag{3}$$

$$\nabla\times\boldsymbol{H}=\boldsymbol{J}, \tag{4}$$

where $\boldsymbol{H}=[H_r, H_z]$ represents the magnetic field components, $\boldsymbol{J}=[J_\varphi]$ represents the current density and $\boldsymbol{E}=[E_\varphi]$ represents the electric field. μ_0 is the permeability of free space and for the superconducting, cold head and vacuum chamber subdomains, the relative permeability is simply $\mu_r=1$.

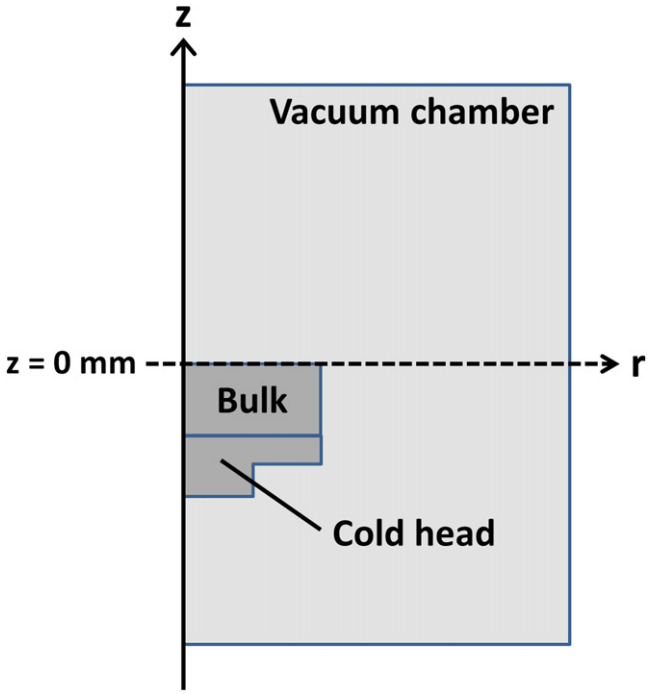

Figure 2. Schematic view of the numerical model of the MgB_2 bulk superconductor, including the cold head and vacuum chamber, for the simulation of FC magnetization.

The temperature-dependence of J_c below T_c is described as equation (5)

$$J_{c0}(T)=\alpha\left[1-\left(\frac{T}{T_c}\right)^2\right]^{1.5}, \tag{5}$$

where α is the critical current density extrapolated to $T=0$ K and $T_c\approx39$ K in the case of MgB_2.

Suitable parameters for the thermal properties must also be assumed for the materials and input into the model. The copper cold head is assumed to have a density of 8940 kg m^{-3}, and a temperature-dependent specific heat and thermal conductivity over the temperature range 0–100 K as given in [33]. For the MgB_2 material, the density is assumed to be 2590 kg m^{-3}, and the specific heat and thermal conductivity for each sample is shown in figures 3 and 5, respectively. All data presented in figures 3 and 5 are measured values from a small sample, except for the specific heat

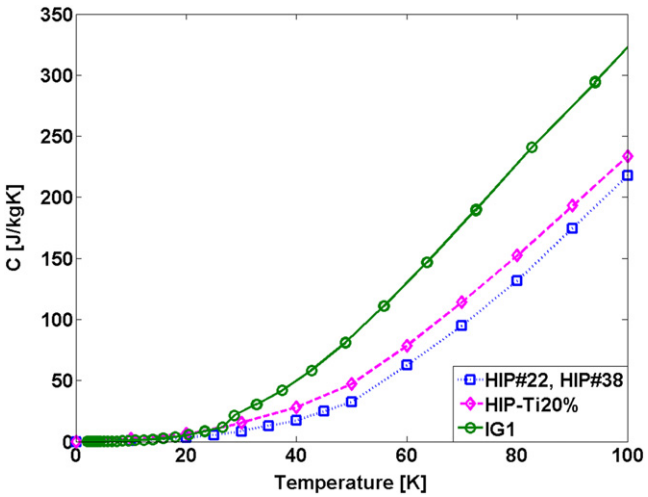

Figure 3. Experimentally measured C (specific heat) data for the HIP#22, HIP#38 and IG1 samples, and the estimated C for the HIP-Ti20% sample.

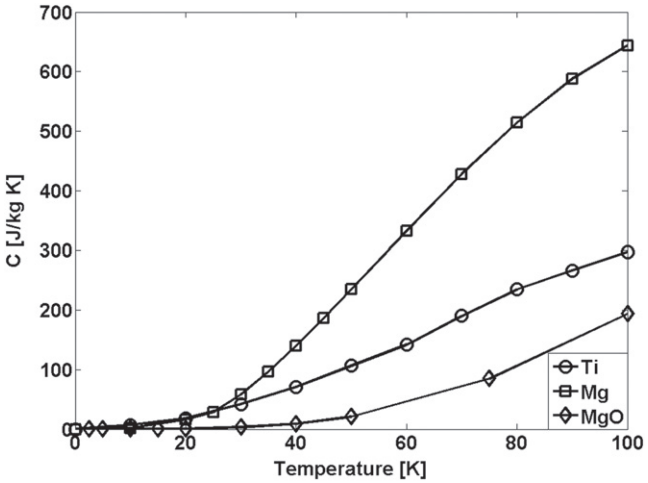

Figure 4. Reference specific heat values for Ti [35], Mg [36] and MgO [37].

for the HIP-Ti20% sample, which is estimated using the specific heat of Ti and the standard HIP samples with a ratio of MgB_2:Ti of 0.8:0.2. This results in a slightly higher specific heat than the undoped samples (HIP#22 and #38, which show good agreement with the classical reference for MgB_2 [34]), due to the presence of Ti, which has a higher specific heat than MgB_2. Reference data for the specific heat of Ti is provided in figure 4 from [35]. These data, as well as the cold head thermal properties, are input into the thermal model using a direct interpolation, similar to a look-up table, in COMSOL.

Interestingly, the specific heat of the IG sample is significantly higher than that of the HIP samples. After processing via IG, there exists a portion of unreacted Mg and MgO in the sample (reference values are 5% MgO and 13% Mg in the sample investigated in [22]) and it is the unreacted Mg that causes an increase in specific heat, due to the significantly higher specific heat of Mg, which is shown in figure 4 from [36]. The specific heat of MgO is slightly lower, but similar to

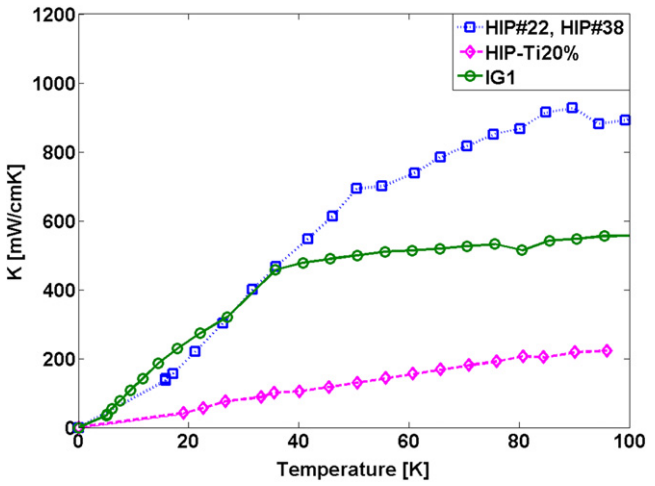

Figure 5. Experimentally measured κ (thermal conductivity) data for the MgB_2 samples.

that of MgB_2, which is also shown for reference in figure 4 from [37].

A suitable approximation must also be made for the $J_c(B, T)$ characteristics of the bulk as shown by equation (6), which was presented in [38, 39]:

$$J_c(B, T) = J_{c0}(T) \exp\left(-\frac{B}{B_0}\right)^a, \tag{6}$$

where B_0 and a are the fitting parameters for each temperature. The measured $J_c(B,T)$ characteristics from a single, small specimen taken from each bulk sample and the estimated curves from the data fitting that are used as input data for the model are shown in figure 6. The data fitting parameters are summarized in table 2.

It is assumed that the electric field $\boldsymbol{E}$ (E_φ) is parallel to the current density $\boldsymbol{J}$ (J_φ) [40, 41] such that $\boldsymbol{J} = \sigma \boldsymbol{E}$ or $\boldsymbol{E} = \rho \boldsymbol{J}$, where σ and ρ are the conductivity and resistivity, respectively, and both highly nonlinear for the superconductor. The electrical behaviour of the superconducting material is modelled by the E–J power law [42, 43], where E is proportional to J^n, as shown in equation (7).

$$\boldsymbol{E} = \frac{E_0}{J_c(B, T)} \left| \frac{J}{J_c(B, T)} \right|^{n-1} \boldsymbol{J}, \tag{7}$$

where $E_0 = 1\,\mu\mathrm{V\,cm^{-1}}$ is the characteristic electric field and n is an appropriate value for the superconductor (in this modelling work, $n = 21$).

Since the real FC magnetization process is being modelled, and this process involves cooling the bulk in-field from a temperature above its transition temperature, this requires valid information on the superconductor's electromagnetic properties above T_c. In order to avoid non-convergence around the transition temperature, we assume a smooth transition from the superconducting state to normal state, shown as equation (8) [44]

$$\rho(T) = \frac{\rho_{sc} \cdot \rho_{normal}}{\rho_{sc} + \rho_{normal}}, \tag{8}$$

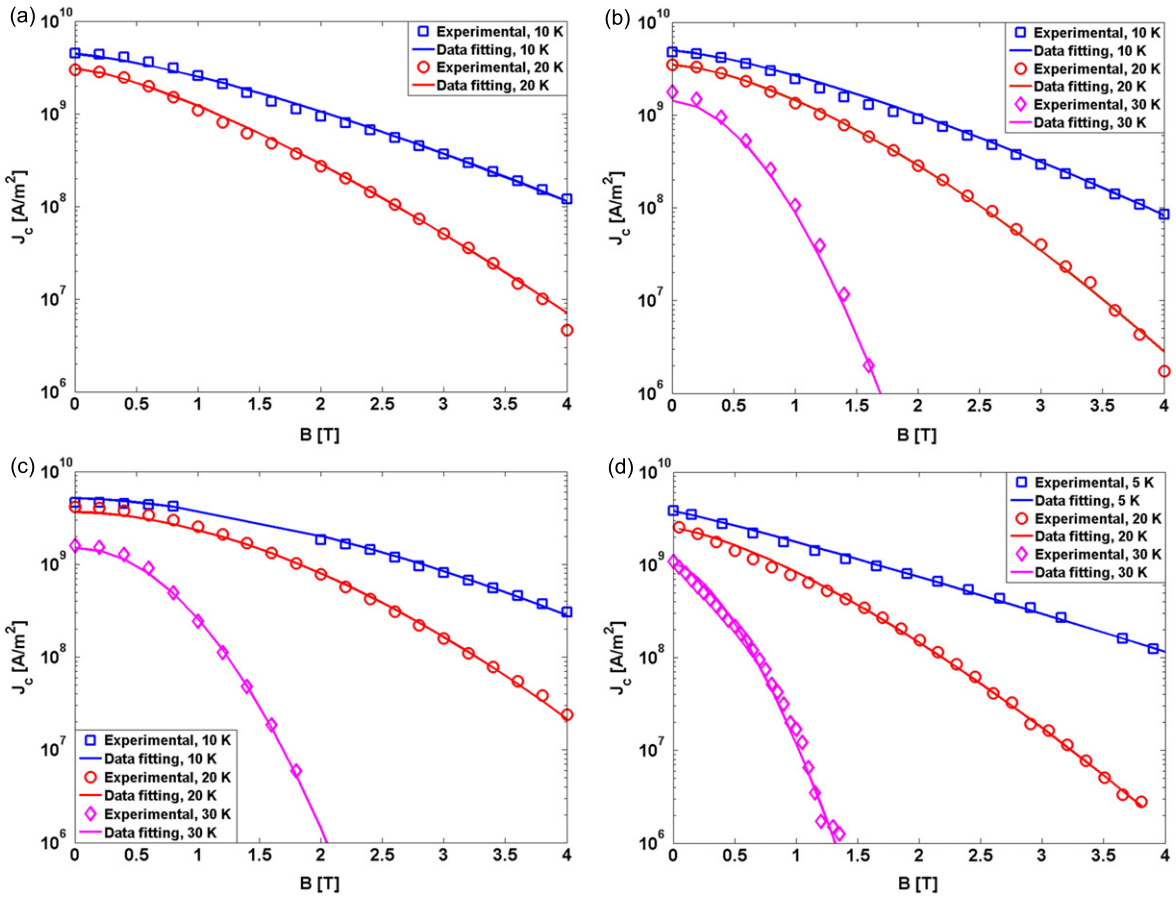

Figure 6. The measured $J_c(B,T)$ characteristics from a single, small specimen taken from each bulk sample and the estimated curves from the data fitting that are used as input data for the models: (a) HIP#22, (b) HIP#38, (c) HIP-Ti20%, and (d) IG1. The data fitting parameters are summarized in table 2.

Table 2. Data fitting parameters for the $J_c(B,T)$ characteristics of each bulk sample based on a single, small specimen.

Sample	T_s	J_{c0} (A m^{-2})	B_0 (T)	a, From equation (6)	α, From equation (5)
HIP#22	10 K	4.42×10^9	1.53	1.35	4.9×10^9
	20 K	3.1×10^9	1.05	1.35	
HIP#38	10 K	4.97×10^9	1.41	1.35	5.5×10^9
	20 K	3.48×10^9	1.09	1.51	
	30 K	1.43×10^9	0.57	1.82	
HIP-Ti20%	10 K	5.24×10^9	2.08	1.63	5.8×10^9
	20 K	3.67×10^9	1.57	1.75	
	30 K	1.51×10^9	0.75	1.98	
IG1	5 K	3.8×10^9	1.27	1.09	3.9×10^9
	20 K	2.47×10^9	0.94	1.38	
	30 K	1.02×10^9	0.39	1.59	

where ρ is the resistivity of the superconductor at any particular temperature, ρ_{normal} is the temperature-dependent resistivity of MgB_2 in the normal state above its transition temperature $T_c \approx 39$ K, and ρ_{sc} is the resistivity below this temperature based on equation (7) and $\boldsymbol{E}=\rho\boldsymbol{J}$. Therefore, when $T<T_c$, the electrical resistivity of the bulk sample in the model tends towards ρ_{sc} and when $T>T_c$, ρ is approximately ρ_{normal}. The details regarding the assumption of the resistivity in the normal state ($\rho_{normal}=3\times10^{-8}\,\Omega$m) can be found in [11].

The simulation of FC magnetization is hence split into three separate time domains:

(1) ($0\leqslant t\leqslant x_1$) Apply a ramped external field to its maximum magnitude (B_{ex}) while the temperature is

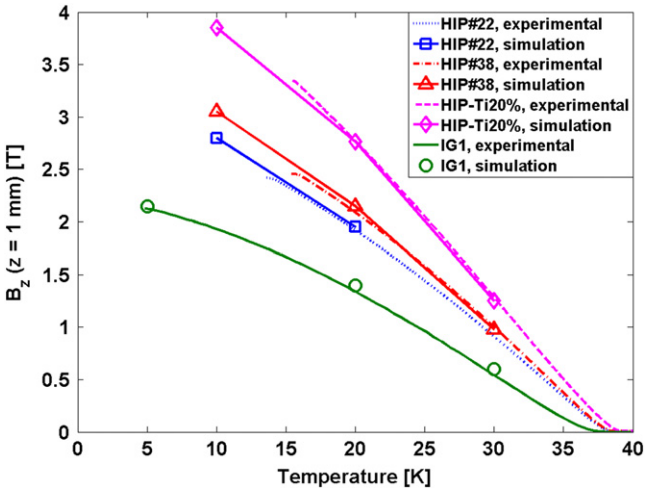

Figure 7. Comparison of the experimental measurements of the trapped field B_z with temperature and the simulation results at 10, 20 and 30 K for the HIP samples and at 5, 20 and 30 K for the IG sample.

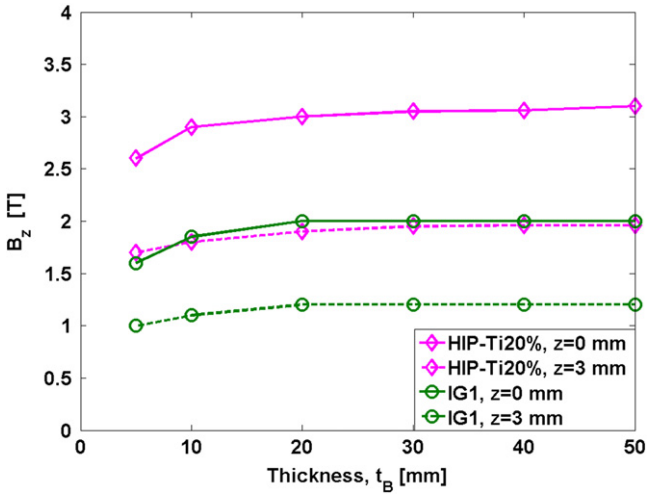

Figure 8. Simulated results for the thickness dependence of the trapped field B_z at the centre of the MgB_2 bulks (HIP-Ti20% and IG1) of diameter 30 mm at $z = 0$ mm (top surface) and $z = 3$ mm at an operating temperature of 20 K.

maintained at T_{ex}, which is larger than T_c ($T_{ex} = 100$ K in this paper)

(2) ($x_1 \leqslant t \leqslant x_2$) Slow cooling of the bulk to an appropriate operating cooling temperature T_{op} (i.e., 30, 20 and 10 K for the HIP samples, and 30, 20 and 5 K for the IG samples). Meanwhile, the external field is held at B_{ex}.

(3) ($x_2 \leqslant t \leqslant x_3$) Once the operating cooling temperature has stabilized, slowly ramp the applied field down from B_{ex} down to 0 T.

This 2D asymmetric model in this case is essentially a reverse-engineered superconducting fault current limiter model with appropriate modifications, and the modelling framework allows for FC magnetization, but can be easily adapted for ZFC and PFM, which are described separately in [30] and [24], respectively.

3.2. Comparison of experimental and simulation results

Figure 7 shows a comparison of the simulation results with the temperature variation of the experimentally measured trapped field, B_z, at a height of $z = 1$ mm above the centre of the bulk surface. In the simulation, an applied field $B_{ex} = 5$ T was applied to each sample to replicate the same experimental conditions under which the samples were magnetized (see, for example, [18] for the details of the FC magnetization for the HIP samples). The time domains (see section 3.1) were split using $x_1 = 2$ s, $x_2 = 60$ s, $x_3 = 180$ s; this corresponds to a ramp down rate of the applied field of 41.67 mT s^{-1}. The simulation reproduces the experimental results extremely well, and additionally, the fact that the experimental results can be reproduced with only a single, small specimen taken from each bulk sample indicates that all of the bulk samples have a highly homogeneous J_c distribution.

Two important results can also be observed from the experimental results. Firstly, doping an MgB_2 bulk with Ti significantly increases the J_c of the HIP-processed sample, resulting in a higher trapped field than pristine, undoped samples processed with the same technique. The critical temperature of such samples is also unaffected by the Ti-doping [18]. Secondly, the trapped field of $B_z = 2.12$ T at 5 K and 1.66 T at 15 K for the IG1 sample is the highest reported trapped field in a bulk MgB_2 sample processed by IG.

In the following section, the numerical model is used to investigate the influence of the sample geometry on the trapped field for samples of different diameters and thickness to optimize the samples geometrically.

3.3. Influence of bulk dimensions on trapped field

Using the numerical model in this paper, the trapped field profile can be estimated for both HIP and IG samples of any dimension, based on valid assumptions, without the need for further experiments. Since the HIP-Ti20% sample has the highest trapped field among the HIP-processed bulks, an analysis of the thickness and diameter dependence of the trapped field for the HIP-Ti20% and IG1 samples is carried out for different sample sizes.

Figure 8 shows the thickness dependence of trapped field at the centre at $z = 0$ mm (top surface of the bulk) and at $z = 3$ mm for the HIP-Ti20% and IG1 samples. The diameter of both samples is fixed at 30 mm and the operating temperature is 20 K. For both samples for a fixed diameter, it can be seen that increasing the thickness of the sample results in a slight increase in trapped field, but this saturates as the sample thickness approaches or is greater than the sample diameter, which agrees with experimental results for the (RE)BCO samples analysed in [45]. A similar trend is observed for the trapped field at a distance $z = 3$ mm above the top surface, indicating that improving the J_c of the sample is the most effective method to increase the trapped field as found in [39].

Figure 9 shows the diameter dependence of the trapped field at the centre at $z = 0$ mm and $z = 3$ mm for the same samples with a fixed thickness of 10 mm. Similarly, the

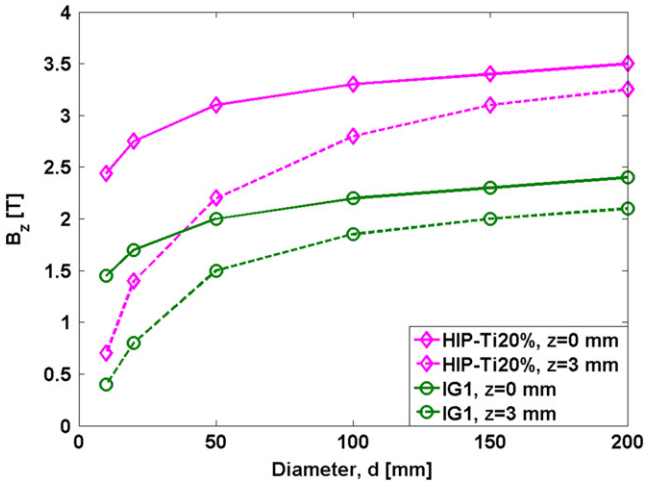

Figure 9. Simulated results for the diameter dependence of the trapped field B_z at the centre of the MgB_2 bulks (HIP-Ti20% and IG1) of thickness 10 mm at $z = 0$ mm (top surface) and $z = 3$ mm at an operating temperature of 20 K.

trapped field increases initially with increasing sample diameter, but saturates when the diameter is several times the thickness. However, increasing the diameter does not result in the same proportional increase in trapped field, which was also concluded in [39]. Based on Bean's model (equation (1)), the trapped field increases linearly by increasing the diameter of the bulk, but this analysis is limited, even when taking into account the geometric factor k given by equation (2), because of the assumption of constant J_c, whereas realistically for the MgB_2 material, and as taken into account in this modelling framework, there is a strong suppression of J_c for increasing magnetic fields. This also leads to the conclusion that enhancing the flux pinning in order to improve the $J_c(B,T)$ characteristics of such bulk superconductors is the most effective method to increase the trapped field.

4. Conclusion

MgB_2 in bulk form shows great promise as TFMs as an alternative to (RE)BCO materials to replace permanent magnets in applications such as rotating machines, magnetic bearings and magnetic separation. In this paper, a comparison is made between bulk MgB_2 samples fabricated by the HIP, with and without Ti-doping, and IG methods and the highest trapped field in an IG-processed bulk MgB_2 sample, $B_z = 2.12$ at 5 K and 1.66 T at 15 K, is reported.

A numerical simulation technique based on the 2D axi-symmetric $\boldsymbol{H}$-formulation is then introduced to model the complete process of FC magnetization, and as input data for the model, the measured $J_c(B,T)$ characteristics of a single, small specimen taken from each bulk sample are used, in addition to measured specific heat and thermal conductivity data for the materials. The results of the simulation reproduce the experimental results extremely well: (1) indicating the samples have excellent homogeneity, and (2) validating the numerical model as a fast, accurate and powerful tool to investigate the superconducting properties and estimate the trapped field profile of bulk MgB_2 discs of any size accurately, under any specific operating conditions.

Finally, the influence of the geometric dimensions of a bulk sample on trapped field is analysed numerically, based on the properties of the HIP-Ti20% and IG1 samples. For a fixed diameter, increasing the thickness of the sample results in a slight increase in trapped field, but this saturates as the sample thickness approaches or is greater than the sample diameter. For a fixed thickness, the trapped field increases initially with increasing sample diameter, but also saturates when the diameter is several times the thickness. Therefore, enhancing the flux pinning in order to improve the $J_c(B,T)$ characteristics of such bulk superconductors is the most effective method to increase the trapped field.

Acknowledgments

JZ would like to acknowledge the support of Churchill College, Cambridge, the China Scholarship Council and the Cambridge Commonwealth, European and International Trust. MA would like to acknowledge the support of a Royal Academy of Engineering Research Fellowship. HF would like to acknowledge support in part by a Grant-in-Aid for Scientific Research from the Ministry of Education, Culture, Sports, Science and Technology, Japan. This research was also supported in part by a Royal Society International Exchanges Scheme grant, IE131084. J-FF would like to thank the Ministry of Higher Education through the Research Council of the University of Liege (Action de Recherches Concertées grant, ARC 11/16-03).

References

[1] Tomita M and Murakami M 2003 *Nature* **421** 517–20
[2] Durrell J H *et al* 2014 *Supercond. Sci. Technol.* **27** 082001
[3] Nariki S, Sakai N and Murakami M 2005 *Supercond. Sci. Technol.* **18** S126–30
[4] Zhou D *et al* 2012 *Supercond. Sci. Technol.* **25** 103001
[5] Hull J R 2000 *Supercond. Sci. Technol.* **13** R1–15
[6] Sino H, Nagashima K and Arai Y 2008 *J. Phys.: Conf. Ser.* **97** 012101
[7] Koshizuka N 2006 *Physica* C **445–448** 1103
[8] Oka T 2007 *Physica* C **463–465** 7
[9] Salama K *et al* 1989 *Appl. Phys. Lett.* **54** 2352–4
[10] Yang W M *et al* 1998 *Physica* C **307** 271–6
[11] Fujishiro H *et al* 2015 *IEEE Trans. Appl. Supercond.* **25** 6800104
[12] Nagamatsu J *et al* 2011 *Nature* **410** 63–4
[13] Xu M *et al* 2001 *Appl. Phys. Lett.* **79** 2779–81
[14] Larbalestier D C *et al* 2001 *Nature* **410** 186–9
[15] Kambara M *et al* 2001 *Supercond. Sci. Technol.* **14** L5
[16] Fuchs G *et al* 2013 *Supercond. Sci. Technol.* **26** 122002
[17] Yamamoto A *et al* 2014 *Appl. Phys. Lett.* **105** 032601
[18] Yoshida T, Naito T and Fujishiro H 2014 *IEEE Trans. Appl. Supercond.* **25** 6801204
[19] Durrell J H *et al* 2012 *Supercond. Sci. Technol.* **25** 112002
[20] Naito T, Sasaki T and Fujishiro H 2012 *Supercond. Sci. Technol.* **25** 095012

[21] Perini E *et al* 2011 *IEEE Trans. Appl. Supercond.* **21** 2690–3
[22] Bhagurkar A G *et al* 2015 *IEEE Trans. Appl. Supercond.* **25** 6801504
[23] Chen D X and Goldfarb R B 1989 *J. Appl. Phys.* **66** 2489
[24] Ainslie M D *et al* 2014 *Supercond. Sci. Technol.* **27** 065008
[25] Bhagurkar A G *et al* 2015 *Supercond. Sci. Technol.* **28** 015012
[26] Fujishiro H *et al* 2011 *Supercond. Sci. Technol.* **24** 105003
[27] Fujishiro H *et al* 2009 *IEEE Trans. Appl. Supercond.* **19** 3545–8
[28] Ainslie M D and Fujishiro H 2015 *Supercond. Sci. Technol.* **28** 053002
[29] Zou J *et al* 2015 *Supercond. Sci. Technol.* **28** 035016
[30] Zou J, Ainslie M D, Hu D and Cardwell D A 2015 *IEEE Trans. Appl. Supercond.* **25** 4900505
[31] Zhang M, Kvitkovic J, Pamidi S V and Coombs T A 2012 *Supercond. Sci. Technol.* **25** 125020
[32] Patel A and Glowacki B A 2012 *Supercond. Sci. Technol.* **25** 125015
[33] Iwasa Y 2009 *Case Studies in Superconducting Magnets: Design and Operational Issues* (New York, USA: Springer Science+Business Media, LLC) pp 354–5
[34] Smith R M and White D 1957 *J. Am. Chem. Soc.* **79** 3641–4
[35] Welsch G, Boyer R and Collings E W 2007 *Materials Properties Handbook: Titanium Alloys* 4th edn (USA: ASM International) p 143
[36] Alcock C B, Chase M W and Itkin V 1993 *J. Phys. Chem. Ref. Data* **22** 1–85
[37] Barron T H K, Berg W T and Morrison J A 1959 *Proc. R. Soc. Ser.* A **250** 70–83
[38] Xiang F X, Wang X L, Xun X, De Silva K S B, Wang Y X and Dou S X 2013 *Appl. Phys. Lett.* **102** 152601
[39] Fujishiro H, Naito T and Yoshida T 2014 *Supercond. Sci. Technol.* **27** 065019
[40] Ainslie M D, Flack T J, Hong Z and Coombs T A 2011 *Int. J. Comput. Math. Electr. Electron. Eng.* **30** 762
[41] Ainslie M D, Rodriguez-Zermeno V M, Hong Z, Yuan W, Flack T J and Coombs T A 2011 *Supercond. Sci. Technol.* **24** 045005
[42] Plummer C J G and Evetts J E 1987 *IEEE Trans. Magn.* **23** 1179–82
[43] Rhyner J 1993 *Physica* C **212** 292–300
[44] Duron J *et al* 2007 *Supercond. Sci. Technol.* **20** 338–44
[45] Fukai H *et al* 2002 *Supercond. Sci. Technol.* **15** 1054–7